Analytical Solution for Thermoelastic Stress Wave Propagation in an Orthotropic Hollow Cylinder

Hamid Sharifi

Louisiana Tech University, Ruston, College of Engineering & Science, Ruston, Louisiana, 71270, USA;
Mechanical Engineering Department, K.N. Toosi University of Technology, Tehran, Iran
E-mail: hsh012@email.latech.edu; hamidsharifyt@alumni.kntu.ac.ir

Received 21 November 2021; Accepted 25 July 2022;
Publication 20 August 2022

Abstract

The problem of thermoelastic stress wave propagation in an orthotropic hollow cylinder is investigated using analytical methods. The fully coupled classical theory of thermoelasticity is used to extract the equations for an orthotropic cylinder. To solve the boundary value problem, heat conduction equation and equation of motion are divided into two different sets of equations, the first set consists of uncoupled equations with considering boundary conditions and the second set comprises coupled ones with initial conditions. Finite Hankel transform (Fourier-Bessel expansion) is utilized to solve the problem with respect to radial variable. Two different cases, pure mechanical load and pure thermal load, were studied numerically to show the effect of considering the thermomechanical coupling term in the heat conduction equation. To show the effect of considering the coupling term in the heat conduction equation, the temperature history is plotted for the pure mechanical load case, where the temperature rises without applying any thermal load. By applying boundary conditions on the inner surface of the

European Journal of Computational Mechanics, Vol. 31_2, 239–274.
doi: 10.13052/ejcm2642-2085.3124

cylinder, initiation of the stress waves from the inner surface of the cylinder, propagation through the thickness in the radial direction and reflection from the outer surface were observed in the plotted figures.

Keywords: Classical thermoelasticity, orthotropic cylinder, Hankel transform, thermoelastic wave.

1 Introduction

Among the different mechanical elements in industries, cylinders are one of the most applicable geometries. Also, using the composite materials in which mechanical properties varies significantly in different directions is growing rapidly due to significant features of these kinds of materials. The composite orthotropic thick walled cylinders are used in a large number of devices such as space crafts, maritime vehicles, etc. Thermal loads are applied on numerous mechanical elements, and the resultant thermal stresses can end to failure of structure. The classical and several generalized theories of thermoelasticity were presented due to the importance of thermal loads in designing structures. The coupled nature of thermoelasticity equations indicates that a change in the temperature field produces a strain and reciprocally, time-dependent deformation causes the change in temperature field. The strain rate term in the energy equation, and the temperature gradient term in the equation of motion are the mathematical indicators of the coupling phenomenon. The coupling terms between these two sets of equations, especially the strain rate term in the energy equation, makes solving the equations of the coupled classical theory of thermoelasticity convoluted, where the both equations must be solved simultaneously. Due to this complications in the equations, analytical solutions have not been developed extensively.

El-Naggar et al. [1] studied thermal stresses in a rotating nonhomogeneous orthotropic hollow cylinder. The problem is considered to be axisymmetric and coupling terms in the heat conduction equation are neglected. They used finite difference method to solve the problem. Shahani and Nabavi [2], used finite Hankel transform to solve quasi-static thermoelasticity problem in a thick hollow isotropic cylinder. The inner and the outer surfaces of the cylinder are subjected to time dependent thermal loadings and two different kinds of mechanical boundary conditions, traction-displacement and traction-traction, are considered to solve the problem. Jabbari et al. [3] presented an exact solution for classical coupled thermoelasticity problem for solid and hollow cylinders. The problem is considered to be radially

symmetric and the cylinder is subjected to mechanical shock and temperature. The Fourier expansion, eigenfunction methods and Laplace transformation are used to solve the equations. Tokovyy and Ma [4] presented an analytical solution to the axisymmetric thermoelasticity for an inhomogeneous layer. They used direct integration and resolvent-kernel technique to obtain closed form analytical solution. The problem is considered to be uncoupled and steady state.

Shahani and Momeni [5] presented analytical solution for thermoelasticity problem in a thick walled isotropic sphere. For solving the both quasi-static and uncoupled dynamic problems a constant temperature is prescribed on the inner boundary, and the inner and the outer surfaces of the sphere are traction free. The boundary conditions are considered to be time-dependent to obtain closed form relations for temperature filed and stress components. They [6] also solved the coupled thermoelasticity problem in a thick walled isotropic sphere. Likewise the previous work, analytical methods are used to solve the problem and closed-form relations are extracted for temperature distribution and the stress field components.

Mahmoudi and Atefi [7] obtained an analytical solution for thermal stresses in a short hollow isotropic cylinder. The inner surface of the cylinder is subjected to a time dependent thermal load, the heat flux is considered to be zero on the outer surface and the both lateral surfaces have constant temperature. They employed Fourier series to solve the problem.

Cho et al. [8] used Laplace transform and Hankel transform to obtain dynamic thermal stresses in a thick orthotropic cylindrical shell. A constant temperature distribution is considered to obtain stress components instead of solving the heat conduction equation. Ding et al. [9]developed a solution for dynamic plane strain thermoelasticity problem for an orthotropic cylinder choosing the same method.

Yun et al. [10] obtained thermal stress distribution in a thick walled cylinder subjected to thermal shock. They used Dirac function to model boundary condition of thermal shock and Laplace transform to solve uncoupled heat conduction equation. The problem is considered to be quasi-static. Dai et al. [11] used finite difference method and Newmark method to analyze dynamic thermoelastic response of long hollow cylinder made of functionally graded materials. The material of the hollow cylinder changes along the radial direction to the power-law distribution.

Tokovyy et al. [12] constructed analytical solution for thermoelasticity problem in a long solid cylinder with varying properties within radial direction. Both Dirichlet and Neumann boundary conditions are considered for

the heat conduction equation. They considered the heat conduction equation in the steady state form. Ying and Wang [13] obtained an exact solution for elastodynamic response of short hollow cylinder subjected to thermal shock based on the uncoupled theory of thermoelasticity. The inner and the outer surfaces of the cylinder are considered to be traction free and the two ends of cylinder are simply-supported. Expansion of trigonometric series method and the separation of variables technique are used to solve the problem.

Nikkhah et al. [14] presented an elastodynamic solution for plane strain response of functionally graded hollow cylinder. To solve the problem, the equation of radial displacement is divided into two quasi-static and dynamic parts and each part is solved analytically. Separation of variables method and the orthogonal expansion technique are used to solve the problem.

Safari-Kahnaki et al. [15] studied thermoelastic stress wave propagation in a functionally graded thick hollow cylinder subjected to thermomechanical shock. The residual theorem and the fast Laplace inverse transform are used to obtain the history of temperature and stress fields. The effects of cylinder thickness and convection heat transfer coefficient on the dynamic behavior of cylinder are discussed.

Vel [16] presented an exact solution for thermoelastic analysis of functionally graded long hollow cylinder. The material is considered to be cylindrical monoclinic and the properties vary as a function of radial coordinate. In addition to the thermal and mechanical boundary conditions on the inner and the outer surfaces, an axial force and torque are applied on the cylinder.

Shahani and Sharifi [17] obtained analytical solution for uncoupled dynamic thermoelasticity problem in an isotropic hollow cylinder. Time-dependent thermal and mechanical boundary conditions are prescribed on the inner and the outer surfaces to present closed form relations for stress components. The finite Hankel transform and Laplace transform are used to solve the problem. They also [18] studied thermal stress wave propagation in an orthotropic hollow cylinder using classical uncoupled dynamic theory of thermoelasticity. An exponentially decaying temperature is applied on the inner surface, and then propagation and reflection of stress wave are studied for two different types of mechanical boundary conditions.

Lata and Kaur [19] presented an investigation on thermomechanical deformation of a homogeneous transversely isotropic thick circular plate. The Laplace and Hankel transforms are used to solve the problem and the inversion of transformations from the transformed domain is obtained numerically. The effects of two temperature thermoelasticity on the deformation of the

plate is also studied. Akbarov and Bagirov [20] investigated the propagation and dispersion of longitudinal elastic waves in a bi-layered hollow cylinder with initial inhomogeneous thermal stresses. The uncoupled classical theory of thermoelasticity is used and the temperature source is heating or cooling of the external free surfaces of the cylinder.

Selvamani et al. [21] used new modified couple stress theory to study wave propagation in a composite hollow circular cylinder. To investigate the effect of the wave number and the thickness, a different theory of thermoelasticity is utilized and three partial differential equations are solved exactly. Mirparizi et al. [22] studied thermal wave propagation and transient response of functionally graded solid subjected to thermal shock using finite strain theory. They employed the Newmark finite difference and FE methods to investigate the effects of volume fraction.

Sharifi and Shahani [23] solved the classical coupled thermoelasticity for an isotropic hollow cylinder. The problem is solved analytically and the mechanical and the thermal boundary conditions are considered to be time dependent. Combination of finite Hankel transform and Laplace transform is used to solve the partial differential equations.

Jafarzadeh et al. [24] developed a new cylindrical shell super-element with trigonometric shape functions to analyse the thermo-mechanical behavior of thin composite vessels. The problem is formulated based on the classical theory of shells and the efficiency and accuracy of the proposed method are investigated.

Sharifi [25] studied the problem of thermal shock in an orthotropic rotating disk using the Lord-Shulman coupled theory of thermoelasticity. The inner boundary of the disk is constrained and subjected to a heat flux and the outer boundary is traction-free and subjected to a constant temperature. The problem is solved analytically using finite Hankel transform and the effects of the angular velocity and the relaxation time are presented in figures.

To the best knowledge of the author the equations of classical coupled thermoelasticity in orthotropic cylinder have not been extracted and solved yet unlike the physical significance. In this paper coupled thermoelasticity problem in an orthotropic hollow cylinder is solved analytically. For thermal boundary conditions, the inner and the outer surfaces of the cylinder are subjected to temperature which is known as the Dirichlet boundary condition as well as the traction for mechanical boundary conditions which is known as Cauchy boundary condition. The problem is solved using an innovative method combined with the finite Hankel transform. Closed-form relations are extracted for the distribution of temperature and stress fields. Two numerical

examples are studied; pure mechanical load and pure thermal load. Distributions of the temperature field and the stress components are presented as figures for these two numerical examples. Propagation of thermal stress wave was observed after plotting stress components which is a result of considering inertia term in the thermoelasticity equations. To verify the results of this solution, the specific case of a hollow orthotropic cylinder subjected to the uniform constant temperature distribution is considered and the stress components histories are compared with those obtained by Ding et al. [9] which shows full compliance. The main difference between this work and previous papers such as [18] is considering coupling term in the energy equation. Existence of this term in the energy equation makes the problem complicated, but the effect of coupling term can be seen in the pure mechanical load case where a temperature gradient is induced without applying any thermal load.

2 Formulation

A long hollow orthotropic cylinder with inner radius of a and outer radius of b is presumed. The length of the cylinder in the axial direction is sufficient to satisfy the plane strain condition. As well as this, symmetric mechanical and thermal boundary conditions are applied to the cylinder. Due to the symmetry in boundary condition and geometry, stress and strain components become independent of the circumferential coordinate and there is only radial dependence of the temperature and displacement distributions. Hence, the stress-strain components relations are [26]:

$$\begin{bmatrix} \sigma_{rr} \\ \sigma_{\varphi\varphi} \\ \sigma_{zz} \\ \tau_{\varphi z} \\ \tau_{rz} \\ \tau_{r\varphi} \end{bmatrix} = \begin{bmatrix} c_{11} & c_{12} & c_{13} & 0 & 0 & 0 \\ c_{12} & c_{22} & c_{23} & 0 & 0 & 0 \\ c_{13} & c_{23} & c_{33} & 0 & 0 & 0 \\ 0 & 0 & 0 & c_{44} & 0 & 0 \\ 0 & 0 & 0 & 0 & c_{55} & 0 \\ 0 & 0 & 0 & 0 & 0 & c_{66} \end{bmatrix} \begin{bmatrix} \varepsilon_{rr} - \alpha_r \Delta T \\ \varepsilon_{\varphi\varphi} - \alpha_\varphi \Delta T \\ \varepsilon_{zz} - \alpha_z \Delta T \\ \gamma_{\varphi z} \\ \gamma_{rz} \\ \gamma_{r\varphi} \end{bmatrix} \tag{1}$$

where α_r, α_φ and α_z are thermal expansion coefficients in three different directions and c_{ij} are the elastic constants. c_{ij} and elastic moduli have following relations:

$$c_{11} = \frac{(1 - \nu_{23}\nu_{32})}{1 - \nu_t} E_1; \quad c_{12} = \frac{(\nu_{21} + \nu_{31}\nu_{23})}{1 - \nu_t} E_1;$$

$$c_{22} = \frac{(1-\nu_{13}\nu_{31})}{1-\nu_t}E_2; \quad c_{13} = \frac{(\nu_{31}+\nu_{21}\nu_{32})}{1-\nu_t}E_1;$$
$$c_{33} = \frac{(1-\nu_{12}\nu_{21})}{1-\nu_t}E_3; \quad c_{23} = \frac{(\nu_{32}+\nu_{12}\nu_{31})}{1-\nu_t}E_2;$$
$$c_{44} = G_{23}; \quad c_{55} = G_{13}; \quad c_{66} = G_{12}; \tag{2}$$

where ν_{ij} are the Poisson's ratios and ν_t is:

$$\nu_t = \nu_{12}\nu_{21} + \nu_{23}\nu_{32} + \nu_{13}\nu_{31} + \nu_{12}\nu_{23}\nu_{31} + \nu_{21}\nu_{32}\nu_{13} \tag{3}$$

where 1, 2 and 3 portray r, φ and z directions, respectively. Due to symmetry in geometry and boundary conditions, it can be concluded that $\tau_{r\varphi} = \tau_{rz}{=}\tau_{z\varphi}{=}\ 0$, and so, the equations of motion reduce to:

$$\frac{\partial \sigma_{rr}}{\partial r} + \frac{1}{r}\left(\sigma_{rr} - \sigma_{\varphi\varphi}\right) = \boldsymbol{\rho}\ddot{u} \tag{4}$$

where ρ is the density. The strain components can be expressed as a function of the radial displacement u in the following form:

$$\varepsilon_{rr} = \frac{\partial u}{\partial r}; \quad \varepsilon_{\varphi\varphi} = \frac{u}{r}; \quad \varepsilon_{\varphi z} = \varepsilon_{zr} = \varepsilon_{r\varphi} = 0 \tag{5}$$

The equation of motion can be extracted in terms of radial displacement by using Equation (5) and Equation (1) and substituting them into Equation (4):

$$\frac{\partial^2 u}{\partial r^2} + \frac{1}{r}\frac{\partial u}{\partial r} - \frac{c_{22}}{c_{11}}\frac{u}{r^2} - \frac{\beta_{11}}{c_{11}}\frac{\partial \theta}{\partial r} + \frac{1}{r}\theta\left(\frac{\beta_{22}-\beta_{11}}{c_{11}}\right) = \frac{\rho}{c_{11}}\ddot{u} \tag{6}$$

where:

$$\beta_{11} = c_{11}\alpha_r + c_{12}\alpha_\varphi + c_{13}\alpha_z \tag{7}$$
$$\beta_{22} = c_{12}\alpha_r + c_{22}\alpha_\varphi + c_{23}\alpha_z \tag{8}$$

and

$$\theta = T(r,t) - T_0 \tag{9}$$

in T_0 the cylinder is stress free. The energy equation in the indicial form is:

$$k_{ij}T_{,ij} - \rho c\dot{T} - T_0\beta_{ij}\dot{\varepsilon}_{ij} = -W \tag{10}$$

where W is the internal heat generation. Due to considering boundary conditions to be axisymmetric, expanding Equation (10) leads to:

$$k\nabla^2 T - \rho c\dot{T} - T_0\beta_{11}\dot{\varepsilon}_{11} - T_0\beta_{22}\dot{\varepsilon}_{22} = -W \tag{11}$$

Neglecting internal heat generation, using Laplace operator in the cylindrical coordinate and Equations (5) and (8), the energy equation reduces to:

$$k\left(\frac{\partial^2\theta}{\partial r^2} + \frac{1}{r}\frac{\partial\theta}{\partial r}\right) - \rho c\frac{\partial\theta}{\partial t} - T_0\beta_{11}\left(\frac{\partial\dot{u}}{\partial r}\right) - T_0\beta_{22}\left(\frac{\dot{u}}{r}\right) = 0 \tag{12}$$

in which k is the thermal conduction coefficient in radial direction and c is the specific heat. Thus, the equations of the coupled thermoelasticity in an orthotropic hollow cylinder are:

$$\frac{\partial^2\theta}{\partial r^2} + \frac{1}{r}\frac{\partial\theta}{\partial r} - \frac{1}{\alpha^*}\frac{\partial\theta}{\partial t} - T_0\frac{\beta_{11}}{k}\left(\frac{\partial\dot{u}}{dr}\right) - T_0\frac{\beta_{22}}{k}\left(\frac{\dot{u}}{r}\right) = 0 \tag{13}$$

$$\frac{\partial^2 u}{\partial r^2} + \frac{1}{r}\frac{\partial u}{\partial r} - \frac{\nu^2}{r^2}u - \frac{\beta_{11}}{c_{11}}\frac{\partial\theta}{\partial r} + \frac{1}{r}\theta\left(\frac{\beta_{22}-\beta_{11}}{c_{11}}\right) = \gamma^2\ddot{u} \tag{14}$$

where:

$$\alpha^* = \frac{k}{\rho c} \tag{15}$$

$$\nu^2 = \frac{c_{22}}{c_{11}} \tag{16}$$

$$\gamma^2 = \frac{\rho}{c_{11}} \tag{17}$$

The last two terms of Equation (13) which include the strain rates, are the thermo-mechanical coupling terms. These terms and the last two terms of the left hand side of Equation (14) are the reason of interaction between thermal and mechanical fields. The radial and hoop stress components, σ_{rr} and $\sigma_{\theta\theta}$ are related to the radial displacement and the temperature field as follows:

$$\sigma_{rr} = c_{11}\frac{\partial u}{\partial r} + c_{12}\frac{u}{r} - \beta_{11}\theta \tag{18}$$

$$\sigma_{\theta\theta} = c_{12}\frac{\partial u}{\partial r} + c_{22}\frac{u}{r} - \beta_{22}\theta \tag{19}$$

The thermal boundary conditions which are prescribed on the inner and the outer surfaces of the cylinder are:

$$\theta(a,t) = f(t) \tag{20}$$

$$\theta(b,t) = g(t) \tag{21}$$

where $f(t)$ and $g(t)$ are known time-dependent functions. The thermal initial condition of the cylinder is:

$$\theta(r,0) = F_1(r) \tag{22}$$

As the mechanical boundary conditions, tractions are applied on both the inner and the outer surfaces of the cylinder:

$$\sigma_{rr}(a,t) = P_1(t) \tag{23}$$

$$\sigma_{rr}(b,t) = P_2(t) \tag{24}$$

By substituting (23) and (24) in (18), we have:

$$\left.\frac{\partial u}{\partial r}\right|_{r=a} + h_1 u(a,t) = B_1(t) \tag{25}$$

$$\left.\frac{\partial u}{\partial r}\right|_{r=b} + h_2 u(b,t) = B_2(t) \tag{26}$$

where:

$$h_1 = \frac{c_{12}}{c_{11}a} \tag{27}$$

$$h_2 = \frac{c_{12}}{c_{11}b} \tag{28}$$

$$B_1(t) = \frac{1}{c_{11}} P_1(t) + \frac{\beta_{11}}{c_{11}} f(t) \tag{29}$$

$$B_2(t) = \frac{1}{c_{11}} P_2(t) + \frac{\beta_{11}}{c_{11}} g(t) \tag{30}$$

For the radial displacement field, initial conditions are considered in the form of general functions of the radial position as follows:

$$u(r,0) = F_2(r) \tag{31}$$

$$\dot{u}(r,0) = F_3(r) \tag{32}$$

and a dot over the quantity is the partial derivative of it with respect to time.

3 The Method of Solution

To solve the coupled thermoelasticity equations, $\theta(r,t)$ and $u(r,t)$ are resolved into two components:

$$u(r,t) = u_1(r,t) + u_2(r,t) \tag{33}$$

$$\theta(r,t) = \theta_1(r,t) + \theta_2(r,t) \tag{34}$$

Applying Equation (34), the boundary value problem related to Equations (13), (20) to (22) are resolved into the following two separate boundary value problems:

$$\frac{\partial^2\theta_1}{\partial r^2} + \frac{1}{r}\frac{\partial\theta_1}{\partial r} - \frac{1}{\alpha^*}\frac{\partial\theta_1}{\partial t} = 0 \tag{35}$$

$$\theta_1(a,t) = f(t) \tag{36}$$

$$\theta_1(b,t) = g(t) \tag{37}$$

$$\theta_1(r,0) = 0 \tag{38}$$

and

$$\frac{\partial^2\theta_2}{\partial r^2} + \frac{1}{r}\frac{\partial\theta_2}{\partial r} - \frac{1}{\alpha^*}\frac{\partial\theta_2}{\partial t} - T_0\frac{\beta_{11}}{k}\left(\frac{d\dot{u}}{dr}\right) - T_0\frac{\beta_{22}}{k}\left(\frac{\dot{u}}{r}\right) = 0 \tag{39}$$

$$\theta_2(a,t) = 0 \tag{40}$$

$$\theta_2(b,t) = 0 \tag{41}$$

$$\theta_2(r,0) = F_1(r) \tag{42}$$

In the same way, Equations (14), (25) and (26) can be resolved into the following boundary value problems by applying the Equation (33):

$$\frac{\partial^2 u_1}{\partial r^2} + \frac{1}{r}\frac{\partial u_1}{\partial r} - \frac{\nu^2}{r^2}u_1 - \gamma^2\ddot{u}_1 = 0 \tag{43}$$

$$\frac{\partial u_1}{\partial r}|_{r=a} + h_1 u_1(a,t) = B_1(t) \tag{44}$$

$$\frac{\partial u_1}{\partial r}|_{r=b} + h_2 u_1(b,t) = B_2(t) \tag{45}$$

$$u_1(r,0) = 0 \tag{46}$$

$$\dot{u}_1(r,0) = 0 \tag{47}$$

and

$$\frac{\partial^2 u_2}{\partial r^2} + \frac{1}{r}\frac{\partial u_2}{\partial r} - \frac{\nu^2}{r^2}u_2 - \gamma^2 \ddot{u}_2 = \frac{\beta_{11}}{c_{11}}\frac{\partial \theta}{\partial r} - \frac{1}{r}\theta\left(\frac{\beta_{22}-\beta_{11}}{c_{11}}\right) \tag{48}$$

$$\left.\frac{\partial u_2}{\partial r}\right|_{r=a} + h_1 u_2(a,t) = 0 \tag{49}$$

$$\left.\frac{\partial u_2}{\partial r}\right|_{r=b} + h_2 u_2(b,t) = 0 \tag{50}$$

$$u_2(r,0) = F_2(r) \tag{51}$$

$$\dot{u}_2(r,0) = F_3(r) \tag{52}$$

The Equations (35) to (38) and (43) to (47) can be solved using the finite Hankel transform [27]:

$$H[\theta_1(r,t);\zeta_n] = \overline{\theta}_1(\zeta_n,t) = \int_a^b r\theta_1(r,t)K_1(\zeta_n,r)dr \tag{53}$$

$$H[u_1(r,t);\xi_m] = \overline{u}_1(\xi_m,t) = \int_a^b r u_1(r,t)K_2(\xi_m,r)dr \tag{54}$$

where $K_1(\zeta_n,r)$ and $K_2(\xi_m,r)$ are the kernels of the transformation. The proper kernel of transformation depends on the general form of the equations and the boundary conditions. For the present problem the kernels of transformations are as follows [28]:

$$K_1(r,\zeta_n) = \mathrm{J}_0(\zeta_n r)\mathrm{Y}_0(\zeta_n R_i) - \mathrm{J}_0(\zeta_n R_i)\mathrm{Y}_0(\zeta_n r) \tag{55}$$

$$\begin{aligned} K_2(r,\xi_m) = {} & \{\mathrm{J}_\nu(\xi_m r)[\xi_m \mathrm{Y}'_\nu(\xi_m a) + h_1 \mathrm{Y}_\nu(\xi_m a)] \\ & - \mathrm{Y}_\nu(\xi_m r)[\xi_m\, \mathrm{J}'_\nu(\xi_m a) + h_1 \mathrm{J}_\nu(\xi_m a)]\} \end{aligned} \tag{56}$$

where ζ_n and ξ_m are the positive roots of the following characteristics equations:

$$\mathrm{J}_0(\zeta_n b)\mathrm{Y}_0(\zeta_n a) - \mathrm{J}_0(\zeta_n a)\mathrm{Y}_0(\zeta_n b) = 0 \tag{57}$$

$$\begin{aligned} & [\xi_m \mathrm{Y}'_\nu(\xi_m a) + h_1 \mathrm{Y}_\nu(\xi_m a)][\xi_m \mathrm{J}'_\nu(\xi_m b) + h_2 \mathrm{J}_\nu(\xi_m b)] \\ & \quad - [\xi_m \mathrm{Y}'_\nu(\xi_m b) + h_2 \mathrm{Y}_\nu(\xi_m b)] \\ & \quad \times [\xi_m\, \mathrm{J}'_\nu(\xi_m a) + h_1 \mathrm{J}_\nu(\xi_m a)] = 0 \end{aligned} \tag{58}$$

The inverse transforms are defined as [28]:

$$H^{-1}[\overline{\theta}_1(\zeta_n,t);r] = \theta_1(r,t) = \sum_{n=1}^{\infty} a_n \overline{\theta}_1(\zeta_n,t)K_1(r,\zeta_n) \tag{59}$$

$$H^{-1}[\overline{u}_1(\xi_m,t);r] = u_1(r,t) = \sum_{m=1}^{\infty} b_m \overline{u}_1(\xi_m,t) K_2(r,\xi_m) \tag{60}$$

where:

$$\begin{aligned} a_n &= \frac{1}{\int_a^b r K_1^2(r,\zeta_n)dr} \\ &= \frac{\pi^2}{2} \frac{\zeta_n^2 \{\mathrm{J}_0(\zeta_n b)\}^2}{\{\mathrm{J}_0(\zeta_n a)\}^2 - \{\mathrm{J}_0(\zeta_n b)\}^2} \end{aligned} \tag{61}$$

$$\begin{aligned} b_m &= \frac{1}{\int_a^b r K_2^2(r,\xi_m)dr} \\ &= \frac{\pi^2 \xi_m^2 e_2^2}{2\{(h_2^2 + \xi_m^2[1-(\frac{\nu}{\xi_m b})^2])e_1^2 - (h_1^2 + \xi_m^2[1-(\frac{\nu}{\xi_m a})^2])e_2^2\}} \end{aligned} \tag{62}$$

in which

$$e_1 = \xi_m \mathrm{J}'_\nu(\xi_m a) + h_1 \mathrm{J}_\nu(\xi_m a) \tag{63}$$

$$e_2 = \xi_m \mathrm{J}'_\nu(\xi_m b) + h_2 \mathrm{J}_\nu(\xi_m b) \tag{64}$$

Applying the finite Hankel transform to the Equations (35) and (43), yields:

$$\frac{\partial \overline{\theta}_1(\zeta_n,t)}{\partial t} + \alpha^* \zeta_n^2 \overline{\theta}_1(\zeta_n,t) = \alpha^* \left[\frac{2\mathrm{J}_0(\zeta_n a)}{\pi \mathrm{J}_0(\zeta_n b)} g(t) - \frac{2}{\pi} f(t) \right] = A_1(t) \tag{65}$$

$$\frac{\partial^2 \overline{u}_1(\xi_m,t)}{\partial t^2} + \left(\frac{\xi_m}{\gamma} \right)^2 \overline{u}_1(\xi_m,t) = \frac{1}{\gamma^2} \left[\frac{2e_1}{\pi e_2} B_2(t) - \frac{2}{\pi} B_1(t) \right] = A_2(t) \tag{66}$$

Equations (65) and (66) are non-homogeneous ordinary differential equations. The solutions of these kinds of equations can be easily obtained as follows:

$$\overline{\theta}_1(\zeta_n,t) = \int_0^t A_1(\tau) e^{-\alpha^* \zeta_n^2 (t-\tau)} d\tau \tag{67}$$

$$\overline{u}_1(\xi_m,t) = \frac{\gamma}{\xi_m} \int_0^t A_2(\tau) \sin\left(\frac{\xi_m}{\gamma}(t-\tau) \right) d\tau \tag{68}$$

Using the inversion relations, Equations (59) and (60) we have:

$$\theta_1(r,t) = \sum_{n=1}^{\infty} a_n K_1(r,\zeta_n) \int_0^t A_1(\tau) e^{-\alpha^* \zeta_n^2 (t-\tau)} d\tau \tag{69}$$

$$u_1(r,t) = \sum_{m=1}^{\infty} \frac{\gamma}{\xi_m} b_m K_2(r,\xi_m) \int_0^t A_2(\tau) \sin\left(\frac{\xi_m}{\gamma}(t-\tau)\right) d\tau \tag{70}$$

As is seen, the first set of the equations have been solved. The following forms are considered for $\theta_2(r,t)$ and $u_2(r,t)$ to solve the second set of the equations [6]:

$$\theta_2(r,t) = \sum_{n=1}^{\infty} Q(t) K_1(r,\zeta_n) \tag{71}$$

$$u_2(r,t) = \sum_{m=1}^{\infty} S(t) K_2(r,\xi_m) \tag{72}$$

where $Q(t)$ and $S(t)$ are unknown functions of time. It should be emphasized that, the above forms for $\theta_2(r,t)$ and $u_2(r,t)$ satisfy the related boundary conditions hence (49) and (50). Substituting Equations (59), (70), (71) and (72) into (39) and (48) yields:

$$\begin{aligned}
&(\dot{Q} + \alpha^* {\zeta_n}^2 Q) K_1(r,\zeta_n) \\
&\quad = -\frac{\alpha^* T_0}{k} (b_m \dot{\overline{u}}_1 + \dot{S}) \\
&\qquad \times \left[\beta_{11} \left(\frac{\partial K_2(r,\xi_m)}{\partial r}\right) + \beta_{22} \left(\frac{K_2(r,\xi_m)}{r}\right)\right]
\end{aligned} \tag{73}$$

$$\begin{aligned}
&\left(\ddot{S} + \left(\frac{\xi_m}{\gamma}\right)^2 S\right) K_2(r,\xi_m) \\
&\quad = -\frac{1}{\gamma^2} \left[\frac{\beta_{11}}{c_{11}} \frac{\partial K_1(r,\zeta_n)}{\partial r} - \frac{1}{r}\left(\frac{\beta_{22}-\beta_{11}}{c_{11}}\right) K_1(r,\zeta_n)\right] \\
&\qquad \times (a_n \overline{\theta}_1 + Q)
\end{aligned} \tag{74}$$

The orthogonality of the Bessel functions are obtained as follows [27]:

$$\int_a^b rK_1(r,\zeta_n)K_1(r,\zeta_p)dr = N_n\delta_{np} \tag{75}$$

$$\int_a^b rK_2(r,\xi_m)K_2(r,\xi_p)dr = M_m\delta_{mp} \tag{76}$$

where δ is the Kronecker delta and:

$$N_n = \frac{\pi^2}{2}\frac{{\zeta_n}^2\{\mathrm{J}_0(\zeta_n b)\}^2}{\{\mathrm{J}_0(\zeta_n a)\}^2 - \{\mathrm{J}_0(\zeta_n b)\}^2} \tag{77}$$

$$M_m = \frac{1}{\xi_m^2}\left\{b^2\frac{dk_2}{dr}\bigg|_{r=b}^2 - a^2\frac{dk_2}{dr}\bigg|_{r=a}^2 + (\xi_m^2-1)\left[b^2k_2^2(b) - a^2k_2^2(a)\right]\right\} \tag{78}$$

Multiplying Equation (36a) by $rK_1(r,\zeta_n)$ and Equation (36b) by $rK_2(r,\xi_m)$, integrating between a and b, and then using the orthogonality relations, result in:

$$\dot{Q} + \alpha^*{\zeta_n}^2 Q = \left\{\begin{array}{l} \alpha^* T_0 \int_a^b rK_1(r,\zeta_n) \\ -\dfrac{\left[\beta_{11}\left(\frac{\partial K_2(r,\xi_m)}{\partial r}\right) + \beta_{22}\left(\frac{K_2(r,\xi_m)}{r}\right)\right]dr}{kN_n} \end{array}\right\} \times (b_m\dot{\overline{u}}_1 + \dot{S}) \tag{79}$$

$$\ddot{S} + \left(\frac{\xi_m}{\gamma}\right)^2 S = \left\{\begin{array}{l} \int_a^b rK_2(r,\xi_m) \\ -\dfrac{\left[\frac{\beta_{11}}{c_{11}}\frac{\partial K_1(r,\zeta_n)}{\partial r} - \frac{1}{r}\left(\frac{\beta_{22}-\beta_{11}}{c_{11}}\right)K_1(r,\zeta_n)\right]dr}{\gamma^2 M_m} \end{array}\right\} \times (a_n\overline{\theta}_1 + Q) \tag{80}$$

The following parameters are defined to simplify above equations:

$$U_1 = \left\{ \begin{array}{c} \alpha^* T_0 \int_a^b r K_1(r,\zeta_n) \\ -\dfrac{\left[\beta_{11}\left(\frac{\partial K_2(r,\xi_m)}{\partial r}\right) + \beta_{22}\left(\frac{K_2(r,\xi_m)}{r}\right)\right] dr}{kN_n} \end{array} \right\} \tag{81}$$

$$U_2 = \left\{ \begin{array}{c} \int_a^b r K_2(r,\xi_m) \\ -\dfrac{\left[\frac{\beta_{11}}{c_{11}}\frac{\partial K_1(r,\zeta_n)}{\partial r} - \frac{1}{r}\left(\frac{\beta_{22}-\beta_{11}}{c_{11}}\right) K_1(r,\zeta_n)\right] dr}{\gamma^2 M_m} \end{array} \right\} \tag{82}$$

Now, Equations (79) and (80) can be written in the simplified form:

$$\dot{Q} + \alpha^* {\zeta_n}^2 Q = U_1(b_m \dot{\bar{u}}_1 + \dot{S}) \tag{83}$$

$$\ddot{S} + \left(\frac{\xi_m}{\gamma}\right)^2 S = U_2(a_n \overline{\theta}_1 + Q) \tag{84}$$

By substituting Equation (42) into (71) the proper form of initial conditions can be obtained:

$$Q(0) K_1(r,\zeta_n) = F_1(r) \tag{85}$$

Using the orthogonality relation (66) leads to:

$$Q(0) = \frac{\int_a^b r K_1(r,\zeta_n) F_1(r) dr}{N_n} \tag{86}$$

The initial conditions for $S(t)$ can be obtained in a similar way:

$$S(0) = \frac{\int_a^b r K_2(r,\xi_m) F_2(r) dr}{M_m} \tag{87}$$

$$\dot{S}(0) = \frac{\int_a^b r K_2(r,\xi_m) F_3(r) dr}{M_m} \tag{88}$$

It is seen that Equations (83) and (84) are coupled. These coupled equations can be uncoupled by some mathematical operations. Differentiating Equations (83) and (84) with respect to time results in:

$$\dddot{Q} + \alpha^* {\zeta_n}^2 \ddot{Q} = U_1(b_m \dddot{\overline{u}}_1 + \dddot{S}) \tag{89}$$

$$\dddot{S} + \left(\frac{\xi_m}{\gamma}\right)^2 \dot{S} = U_2(a_n \dot{\overline{\theta}}_1 + \dot{Q}) \tag{90}$$

Substituting $\dot{Q}$ from Equation (83) in the Equation (90) leads to:

$$\dddot{S} + \left(\frac{\xi_m}{\gamma}\right)^2 \dot{S} = U_2[a_n \dot{\overline{\theta}}_1 + U_1(b_m \dot{\overline{u}}_1 + \dot{S}) - \alpha^* {\zeta_n}^2 Q] \tag{91}$$

Now by substituting Q from Equation (84) into Equation (91) we have:

$$\dddot{S} + \left(\frac{\xi_m}{\gamma}\right)^2 \dot{S} = U_2 \Bigg[a_n \dot{\overline{\theta}}_1 + U_1 \left(b_m \dot{\overline{u}}_1 + \dot{S}\right) - \alpha^* {\zeta_n}^2 \left(\frac{1}{U_2}(\ddot{S} + \left(\frac{\xi_m}{\gamma}\right)^2 S) - a_n \overline{\theta}_1\right) \Bigg] \tag{92}$$

As is seen Equation (92) is independent of Q. Substituting $\dddot{S}$ from Equation (89) into Equation (90)leads to:

$$\ddddot{Q} + \alpha^* {\zeta_n}^2 \ddot{Q} = U_1 \left[b_m \dddot{\overline{u}}_1 + U_2(a_n \dot{\overline{\theta}}_1 + \dot{Q}) - \left(\frac{\xi_m}{\gamma}\right)^2 \dot{S} \right] \tag{93}$$

Now by substituting $\dot{S}$ from Equation (83) into Equation (93) we have:

$$\ddddot{Q} + \alpha^* {\zeta_n}^2 \ddot{Q} = U_1 \Bigg[b_m \dddot{\overline{u}}_1 + U_2(a_n \dot{\overline{\theta}}_1 + \dot{Q}) - \left(\frac{\xi_m}{\gamma}\right)^2 \left(\frac{1}{U_1}\left(\dot{Q} + \alpha^* {\zeta_n}^2 Q\right) - b_m \dot{\overline{u}}_1\right) \Bigg] \tag{94}$$

Rewriting Equations (92) and (94), leads to:

$$\frac{d^3 S}{dt^3} + \alpha^* \zeta_n^2 \frac{d^2 S}{dt^2} + \left(\left(\frac{\xi_m}{\gamma}\right)^2 - U_1 U_2\right) \frac{dS}{dt} + \alpha^* \zeta_n^2 \left(\frac{\xi_m}{\gamma}\right)^2 S$$

$$= b_m U_1 U_2 \dot{\overline{u}}_1 + a_n U_2 (\dot{\overline{\theta}}_1 + \alpha^* \zeta_n^2 \overline{\theta}_1) \tag{95}$$

$$\frac{d^3Q}{dt^3} + \alpha^* \zeta_n^2 \frac{d^2Q}{dt^2} + \left(\left(\frac{\xi_m}{\gamma} \right)^2 - U_1 U_2 \right) \frac{dQ}{dt} + \alpha^* \zeta_n^2 \left(\frac{\xi_m}{\gamma} \right)^2 Q$$

$$= b_m U_1 \frac{d}{dt} \left(\ddot{\overline{u}}_1 + \left(\frac{\xi_m}{\gamma} \right)^2 \overline{u}_1 \right) + a_n U_1 U_2 \dot{\overline{\theta}}_1 \tag{96}$$

Equations (95) and (96) are ordinary differential equations. Substituting Equations (65) and (66) into Equations (95) and (96) results in:

$$\frac{d^3S}{dt^3} + \alpha^* \zeta_n^2 \frac{d^2S}{dt^2} + \left(\left(\frac{\xi_m}{\gamma} \right)^2 - U_1 U_2 \right) \frac{dS}{dt} + \alpha^* \zeta_n^2 \left(\frac{\xi_m}{\gamma} \right)^2 S$$

$$= U_2 (b_m U_1 \dot{\overline{u}}_1 + a_n A_1(t)) \tag{97}$$

$$\frac{d^3Q}{dt^3} + \alpha^* \zeta_n^2 \frac{d^2Q}{dt^2} + \left(\left(\frac{\xi_m}{\gamma} \right)^2 - U_1 U_2 \right) \frac{dQ}{dt} + \alpha^* \zeta_n^2 \left(\frac{\xi_m}{\gamma} \right)^2 Q$$

$$= U_1 \left(b_m \dot{A}_2(t) + a_n U_2 \dot{\overline{\theta}}_1 \right) \tag{98}$$

$Q(t, \xi_m)$ and $S(t, \zeta_n)$ can be obtained by solving Equations (97) and (98). The solutions of the Equations (97) and (98), depend on the mechanical and the thermal boundary conditions, thus $Q(t, \xi_m)$ and $S(t, \zeta_n)$ are presented in the numerical examples section. Now, the solutions for both parts of $\theta(r, t)$ and $u(r, t)$ are obtained and the closed form relations for temperature and displacement are:

$$\theta(r,t) = \sum_{n=1}^{\infty} a_n \overline{\theta}_1(t) K_1(r, \zeta_n) + \sum_{m=1}^{\infty} \sum_{n=1}^{\infty} Q(t, \xi_m) K_1(r, \zeta_n) \tag{99}$$

$$u(r,t) = \sum_{m=1}^{\infty} b_m \overline{u}_1(t) K_2(r, \xi_m) + \sum_{m=1}^{\infty} \sum_{n=1}^{\infty} S(t, \zeta_n) K_2(r, \xi_m) \tag{100}$$

4 Numerical Examples

In this section two numerical examples are considered in order to study the response of the orthotropic cylinder under external loads. The following

material properties are employed in the calculations:

$$a = 1 \text{ m};\ b = 2 \text{ m};\ P = 100 \text{ MPa};\ \theta_0 = 100,\ \alpha^* = .112E-6W/m^2K$$
$$E_{11} = 19.8 \text{ GPa};\ E_{22} = 48.3 \text{ GPa};\ E_{33} = 19.8 \text{ GPa};\ G_{12} = 8.9 \text{ GPa};$$
$$G_{23} = 8.9 \text{ GPa};\ G_{31} = 6.19 \text{ GPa};\ \nu_{12} = .27;\ \nu_{23} = .27;\ \nu_{31} = .3$$
$$\alpha_{11} = 15E-6\ 1/K;\ \alpha_{22} = 23E-6\ 1/K;\ \alpha_{33} = 15E-6\ 1/K;$$

4.1 Pure Mechanical Load

In the case when only mechanical load is applied on the inner surface of the cylinder, thermal and mechanical boundary conditions are:

$$\theta(a,t) = 0 \tag{101}$$
$$\theta(b,t) = 0 \tag{102}$$
$$\sigma_{rr}(a,t) = -P \tag{103}$$
$$\sigma_{rr}(b,t) = 0 \tag{104}$$

Thermal and mechanical initial conditions are:

$$\theta(r,0) = 0 \tag{105}$$
$$u(r,0) = 0 \tag{106}$$
$$\dot{u}(r,0) = 0 \tag{107}$$

Thus we have:

$$Q(0) = 0 \tag{108}$$
$$S(0) = 0 \tag{109}$$
$$\dot{S}(0) = 0 \tag{110}$$

Using thermal boundary conditions and Equation (65) we have:

$$A_1(t) = 0 \tag{111}$$
$$\overline{\theta}_1(\zeta_n,t) = 0 \tag{112}$$

Using mechanical boundary conditions and Equations (29) and (30) we have:

$$B_1 = -\frac{1}{c_{11}}P \tag{113}$$

$$B_2 = 0 \tag{114}$$

$$A_2(t) = \frac{2P}{\pi\gamma^2 c_{11}} \tag{115}$$

Substituting Equation (113) into Equation (68) gives:

$$\overline{u}_1(\xi_m, t) = \frac{2P}{\pi\xi_m^2 c_{11}}\left(1 - \cos\left(\frac{\xi_m}{\gamma}t\right)\right) \tag{116}$$

Substituting Equations (112) and (116) into Equations (69) and (70) gives:

$$\theta_1(r,t) = 0 \tag{117}$$

$$u_1(r,t) = \frac{2P}{\pi c_{11}}\sum_{m=1}^{\infty}\frac{b_m}{\xi_m^2}\left(1 - \cos\left(\frac{\xi_m}{\gamma}t\right)\right)K_2(r,\xi_m) \tag{118}$$

This way Equations (88) and (98) yield:

$$\frac{d^3S}{dt^3} + \alpha^*\zeta_n^2\frac{d^2S}{dt^2} + \left(\left(\frac{\xi_m}{\gamma}\right)^2 - U_1U_2\right)\frac{dS}{dt} + \alpha^*\zeta_n^2\left(\frac{\xi_m}{\gamma}\right)^2 S = R\sin\left(\frac{\xi_m}{\gamma}t\right) \tag{119}$$

$$\frac{d^3Q}{dt^3} + \alpha^*\zeta_n^2\frac{d^2Q}{dt^2} + \left(\left(\frac{\xi_m}{\gamma}\right)^2 - U_1U_2\right)\frac{dQ}{dt} + \alpha^*\zeta_n^2\left(\frac{\xi_m}{\gamma}\right)^2 Q = 0 \tag{120}$$

where:

$$R = \frac{2b_m U_1 U_2 P}{\pi\xi_m\gamma c_{11}} \tag{121}$$

Solving Equations (119) and (120) results in:

$$S(t) = \frac{R\gamma}{\xi_m U_1 U_2}\cos\left(\frac{\xi_m}{\gamma}t\right) + \sum_{i=1}^{3} c_i e^{\alpha_i t} \tag{122}$$

$$Q(t) = \frac{1}{U_2}\sum_{i=1}^{3}\left(\alpha_i^2 + \left(\frac{\xi_m}{\gamma}\right)^2\right) c_i e^{\alpha_i t} \tag{123}$$

where α_i's are the roots of following equation:

$$x^3 + \alpha^* {\zeta_n}^2 x^2 + \left(\left(\frac{\xi_m}{\gamma}\right)^2 - U_1 U_2\right) x + \alpha^* {\zeta_n}^2 \left(\frac{\xi_m}{\gamma}\right)^2 = 0 \tag{124}$$

It should be mentioned that $Q(t)$ is obtained by using Equation (84). The constants c_i's can be obtained using Equations (108) to (110).

$$\begin{pmatrix} c_1 \\ c_2 \\ c_3 \end{pmatrix} = \begin{pmatrix} 1 & 1 & 1 \\ \alpha_1 & \alpha_2 & \alpha_3 \\ \alpha_1^2 + \left(\frac{\xi_m}{\gamma}\right)^2 & \alpha_2^2 + \left(\frac{\xi_m}{\gamma}\right)^2 & \alpha_3^2 + \left(\frac{\xi_m}{\gamma}\right)^2 \end{pmatrix}^{-1} \times \begin{pmatrix} -\frac{R\gamma}{\xi_m U_1 U_2} \\ 0 \\ 0 \end{pmatrix} \tag{125}$$

Equation (124) is a cubic equation and has three roots, one of which is a negative real number and the two others are complex conjugate with negative real parts. Because of the negative power of the exponential terms in Equations (122) and (123), they vanish over time passing. In the following figures, history of the stress components and the temperature are shown. Figures 1 and 2 present the history of dynamic radial and hoop stresses.

As it is seen in Figure 1, dilatation wave which initiated at the inner surface of the cylinder, moves forward from the inner surface and after colliding outer surface reflects into the medium in the opposite direction. Due to the traction free boundary condition of the outer surface, the propagated wave becomes reversed after collision by outer surface.

As a matter of fact, compressive radial stress wave produces tensile hoop stress. But as is seen from Figure 2, at the initial moments as the compressive

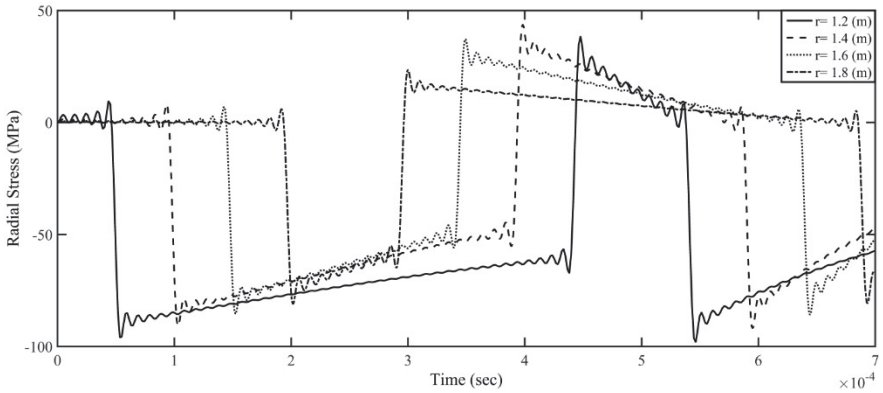

Figure 1 History of dynamic radial stress for different radial positions (case i).

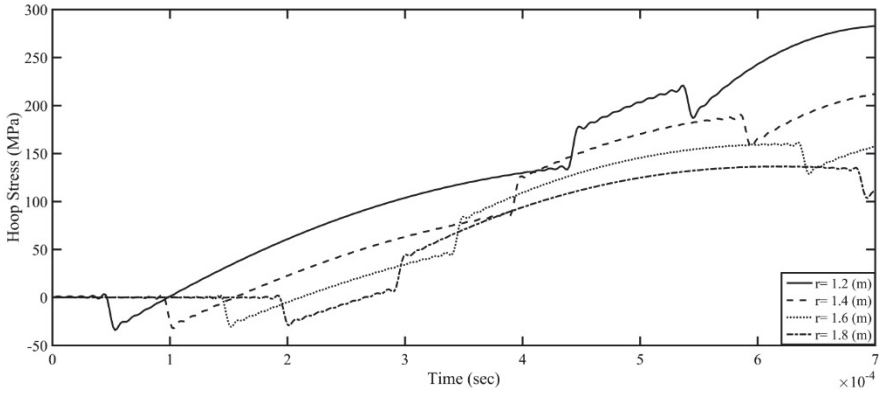

Figure 2 History of dynamic hoop stress for different radial positions (case i).

stress wave reaches any radial position, tangential stress component becomes compressive and then increases gradually with time. The reason of this phenomenon is the resistance of the nearby points in the medium which exerts to any point.

Due to existence of strain rate terms in the energy equation, a change in the amount of strain can produce a temperature change. In this example, there is not any thermal load applied to the cylinder, but because of the coupling term a change in temperature is observed. Figure 3 shows this temperature difference with respect to the reference temperature.

Figures 4 and 5 show through-thickness variation of hoop and radial stresses. Velocity of the propagated wave is the reverse square root of the

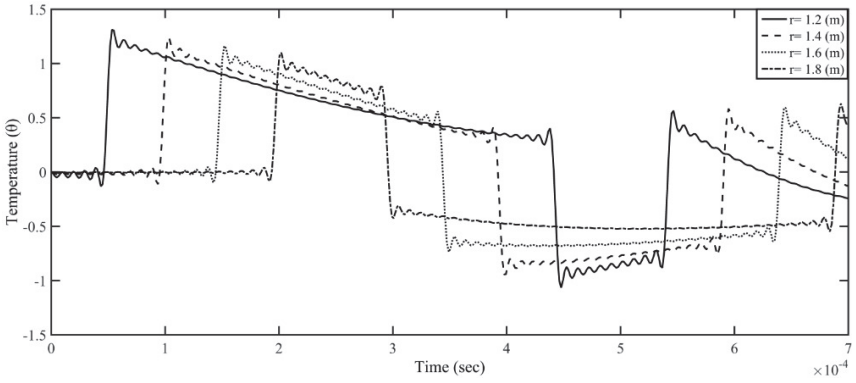

Figure 3 History of temperature for different radial positions (case i).

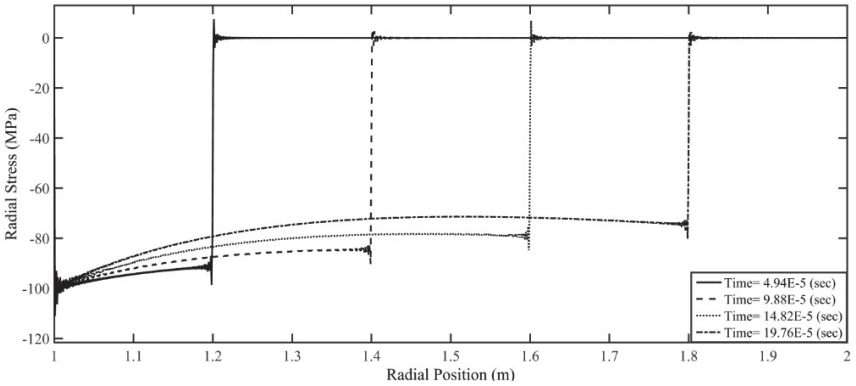

Figure 4 Through-thickness variation of dynamic radial stress (case i).

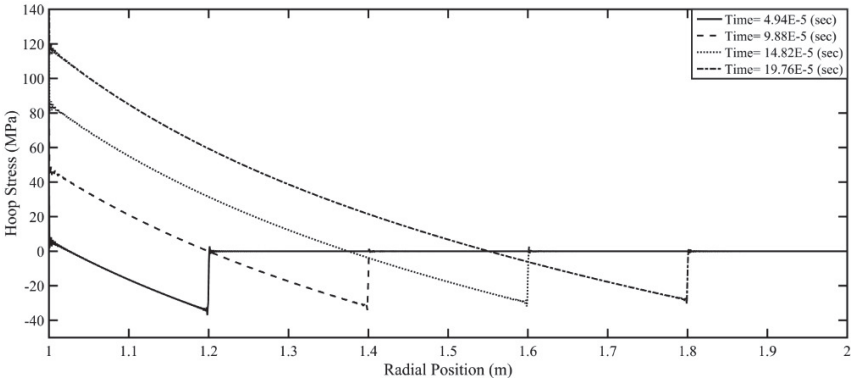

Figure 5 Through-thickness variation of dynamic hoop stress (case i).

factor of the second derivative of displacement respect to the time, in the motion equation and can be obtained using the following equation:

$$V_e = \frac{1}{\gamma} = 4.0493 \times 10^3 (\mathrm{m/s}) \tag{126}$$

The first time dilatation wave reaches to different radial positions can be computed using the velocity of wave. For example:

$$t^* = \frac{r-a}{V_e} = \frac{1.2-1}{4049} = 4.94 \times 10^{-5} (\mathrm{sec}) \tag{127}$$

It is seen from the Figures 4 and 5 that at the same time as computed in Equation (127), the stress wave has been reached the radial position r = 1.2.

As is mentioned due to resistance which exerted to any point by medium, tangential component becomes compressive at the initial moments and then proceeds from negative to positive. This reality is obviously shown in the Figure 5.

4.2 Pure Thermal Load

In this case, it is considered that the inner surface of the cylinder is subjected to a constant temperature. So, thermal and mechanical boundary conditions are:

$$\theta(a,t) = \theta_0 \tag{128}$$

$$\theta(b,t) = 0 \tag{129}$$

$$\sigma_{rr}(a,t) = 0 \tag{130}$$

$$\sigma_{rr}(b,t) = 0 \tag{131}$$

Thermal and mechanical initial conditions are:

$$\theta(r,0) = 0 \tag{132}$$

$$u(r,0) = 0 \tag{133}$$

$$\dot{u}(r,0) = 0 \tag{134}$$

Thus we have:

$$Q(0) = 0 \tag{135}$$

$$S(0) = 0 \tag{136}$$

$$\dot{S}(0) = 0 \tag{137}$$

Using the thermal boundary conditions and Equations (65) and (66) together with Equations (29) and (30), yield:

$$A_1(t) = -\frac{2\alpha^*\theta_0}{\pi} \tag{138}$$

$$A_2(t) = -\frac{2\theta_0\beta_{11}}{\pi\gamma^2 c_{11}} \tag{139}$$

Using Equations (33a) and (33b), leads to:

$$\overline{\theta}_1(\zeta_n, t) = -\frac{2\theta_0}{\pi\zeta_n^2}(1 - e^{-\alpha^*\zeta_n^2 t}) \tag{140}$$

$$\overline{u}_1(\xi_m, t) = -\frac{2\theta_0\beta_{11}}{\pi\xi_m^2 c_{11}}\left(1 - \cos\left(\frac{\xi_m}{\gamma}t\right)\right) \tag{141}$$

Substituting Equations (138) and (139) into Equations (69) and (70), results in:

$$\theta_1(r,t) = -\frac{2\theta_0}{\pi}\sum_{n=1}^{\infty}\frac{a_n}{\zeta_n^2}(1 - e^{-\alpha^*\zeta_n^2 t})K_1(r,\zeta_n) \tag{142}$$

$$u_1(r,t) = -\frac{2\theta_0\beta_{11}}{\pi c_{11}}\sum_{m=1}^{\infty}\frac{b_m}{\xi_m^2}\left(1 - \cos\left(\frac{\xi_m}{\gamma}t\right)\right)K_2(r,\xi_m) \tag{143}$$

Equations (97) and (98) then can be written as:

$$\frac{d^3S}{dt^3} + \alpha^*\zeta_n^2\frac{d^2S}{dt^2} + \left(\left(\frac{\xi_m}{\gamma}\right)^2 - U_1U_2\right)\frac{dS}{dt} + \alpha^*\zeta_n^2\left(\frac{\xi_m}{\gamma}\right)^2 S$$
$$= -U_2\left(b_m U_1\frac{2\theta_0\beta_{11}}{\pi\xi_m\gamma c_{11}}\sin\left(\frac{\xi_m}{\gamma}t\right) + a_n\frac{2\alpha^*\theta_0}{\pi}\right) \tag{144}$$

$$\frac{d^3Q}{dt^3} + \alpha^*\zeta_n^2\frac{d^2Q}{dt^2} + \left(\left(\frac{\xi_m}{\gamma}\right)^2 - U_1U_2\right)\frac{dQ}{dt} + \alpha^*\zeta_n^2\left(\frac{\xi_m}{\gamma}\right)^2 Q$$
$$= -U_1\left(a_n U_2\frac{2\theta_0\alpha^*}{\pi}e^{-\alpha^*\zeta_n^2 t}\right) \tag{145}$$

Solving the above equations, we arrive at:

$$S(t) = -\frac{2a_n\theta_0 U_2}{\pi\zeta_n^2(\frac{\xi_m}{\gamma})^2} - \frac{2b_m\theta_0\beta_{11}}{\pi\xi_m^2 c_{11}}\cos\left(\frac{\xi_m}{\gamma}t\right) + \sum_{i=1}^{3} c_i e^{\alpha_i t} \tag{146}$$

$$Q(t) = -\frac{2a_n\theta_0}{\pi\zeta_n^2}e^{-\alpha^*\zeta_n^2 t} + \frac{1}{U_2}\sum_{i=1}^{3}\left(\alpha_i^2 + \left(\frac{\xi_m}{\gamma}\right)^2\right)c_i e^{\alpha_i t} \tag{147}$$

where α_i's are the roots of Equation (124) and the constants c_i can be obtained using Equations (66) to (68):

$$\begin{pmatrix} c_1 \\ c_2 \\ c_3 \end{pmatrix} = \frac{2\theta_0}{\pi}\begin{pmatrix} 1 & 1 & 1 \\ \alpha_1 & \alpha_2 & \alpha_3 \\ \alpha_1^2 + \left(\frac{\xi_m}{\gamma}\right)^2 & \alpha_2^2 + \left(\frac{\xi_m}{\gamma}\right)^2 & \alpha_3^2 + \left(\frac{\xi_m}{\gamma}\right)^2 \end{pmatrix}^{-1} \times \begin{pmatrix} \frac{a_n U_2}{\zeta_n^2\left(\frac{\xi_m}{\gamma}\right)^2} + \frac{b_m\beta_{11}}{\xi_m^2 c_{11}} \\ 0 \\ \frac{a_n U_2}{\zeta_n^2} \end{pmatrix} \tag{148}$$

The stress components are shown in Figures 6 and 7. Applying thermal load on the inner surface at the earlier moments causes a thermal shock which is observed in figures. Similar to the mechanical load, dilatation wave which is produced at the inner surface moves forward from the inner surface and after colliding outer surface reflects into the medium in the opposite direction.

The temperature field has the exponential distribution with time, and it takes time the thermal load effect reaches any radial position and makes a change in stress components. Contrary to the pure mechanical load case, in the pure thermal load, radial stress wave is tensile and produces compressive hoop stress. When the tensile wave reaches a specific radial position, the tangential stress component also becomes suddenly tensile due to the resistance of the nearby points in the medium and decays gradually with time.

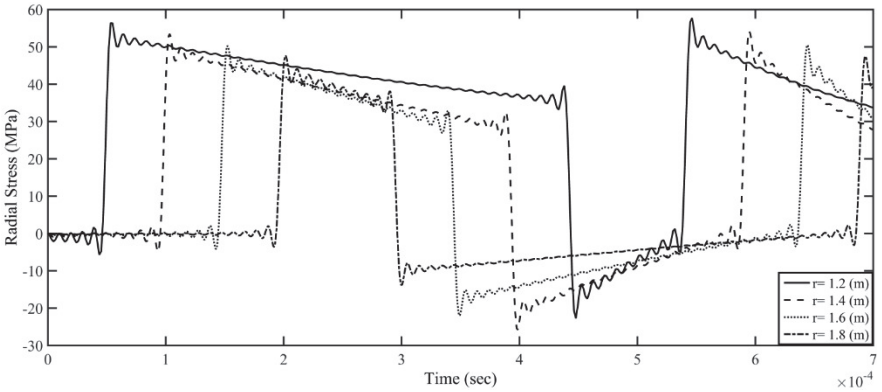

Figure 6 History of dynamic radial stress for different radial positions (case ii).

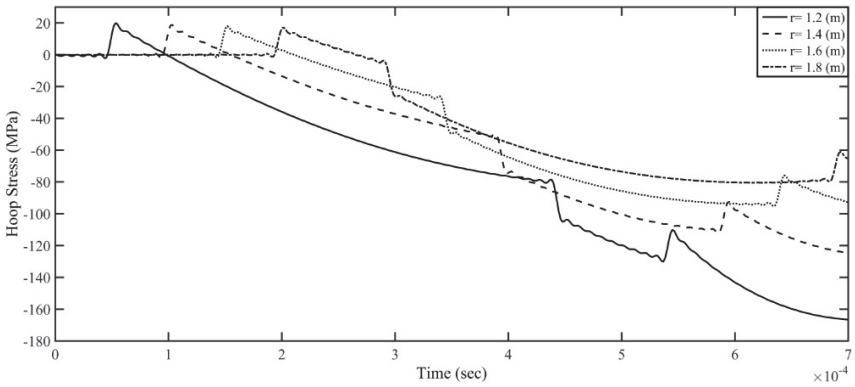

Figure 7 History of dynamic hoop stress for different radial positions (case ii).

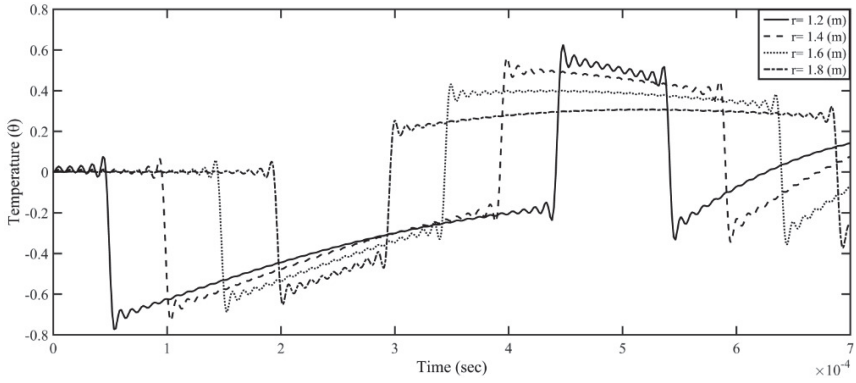

Figure 8 History of temperature for different radial positions (case ii).

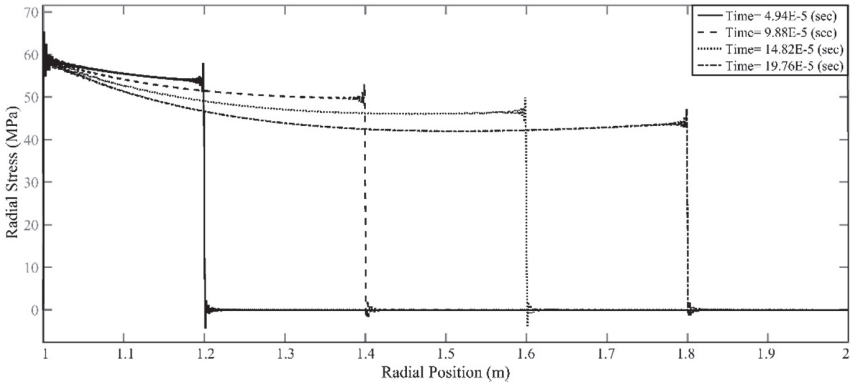

Figure 9 Through-thickness variation of dynamic radial stress (case ii).

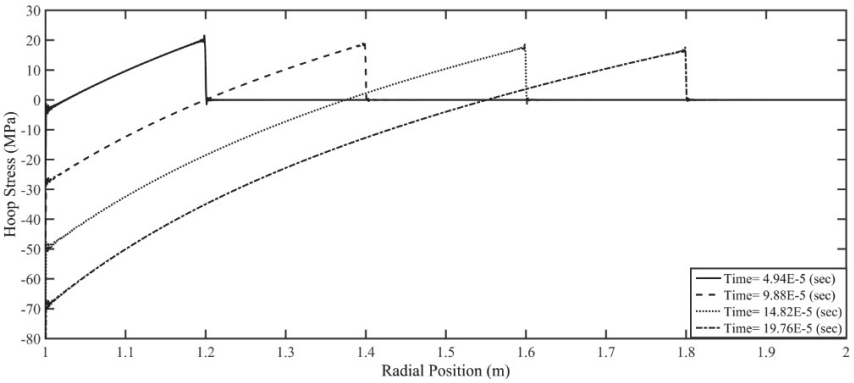

Figure 10 Through-thickness variation of dynamic hoop stress (case ii).

Figure 8 shows the temperature difference with respect to the reference temperature. Due to plotting the figure in short period of time, the coupling effect is the main part of the temperature history. Indeed the figure shows the effect of the coupling terms and there is no trace of the heat conduction mechanism but over time passing the heat conduction becomes the dominant part of the temperature difference distribution and the effect of the coupling terms becomes negligible.

Figures 9 and 10 shows the through-thickness variation of radial and hoop stress components.

As is mentioned, due to resistance of nearby points, tangential component becomes tensile at the initial moments and then proceeds from positive to negative. This reality is obviously shown in the Figure 10.

5 Validation

5.1 Uniformly Heated Orthotropic Cylinder

To validate current work, the special case of dynamic thermal stresses in a hollow orthotropic cylinder subjected to constant temperature distribution is considered. In these kinds of problems, to simplify the solution, a uniform constant temperature is considered for all radial positions instead of solving the heat conduction equation. The history of non-dimensional radial and hoop stresses are plotted in Figures 11 and 12. Due to acting thermo-mechanical loadings on both the inner and the outer surfaces of the cylinder, there are two thermo-elastic waves. The first one propagates from inner surface and the second one initiates from outer surface. The corresponding obtained results by Ding et al. [9] are shown on the same figures. It can be seen that the results of this work are in good agreement with the results of Ding et al. [9]. To calculate the stresses following material properties are employed:

$$a = 50 \text{ mm};\ b = 100 \text{ mm};\ \theta_0 = 200,\ c_{11} = 17.075 \text{ GPa}$$

$$c_{12} = 6.757 \text{ GPa};\ c_{13} = 7.289 \text{ GPa};\ c_{22} = 59.645 \text{ GPa};$$

$$c_{23} = 6.752 \text{ GPa};\ c_{33} = 17.074 \text{ GPa};\ \rho = 1700 \text{ kg/m}^3$$

$$\alpha_{11} = 4E-5\ 1/K;\ \alpha_{22} = 1E-5\ 1/K;\ \alpha_{33} = 4E-5\ 1/K;$$

The following relation is used to make the time dimensionless.

$$\bar{t} = \frac{V_e t}{a} \tag{149}$$

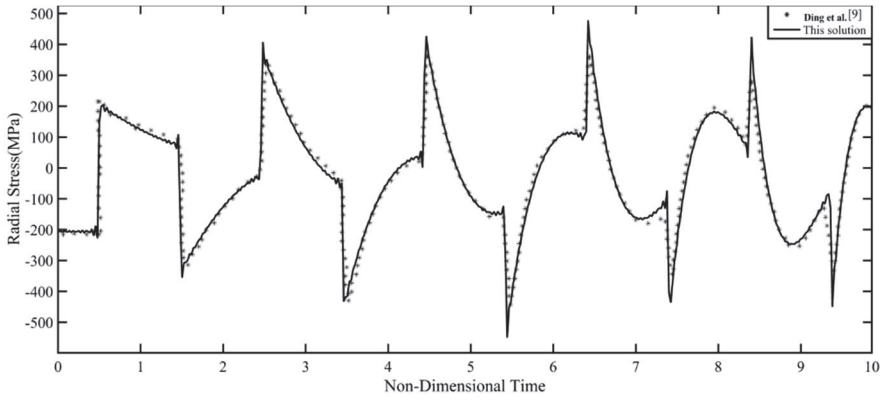

Figure 11 Variation of radial stress for r = (a+b)/2.

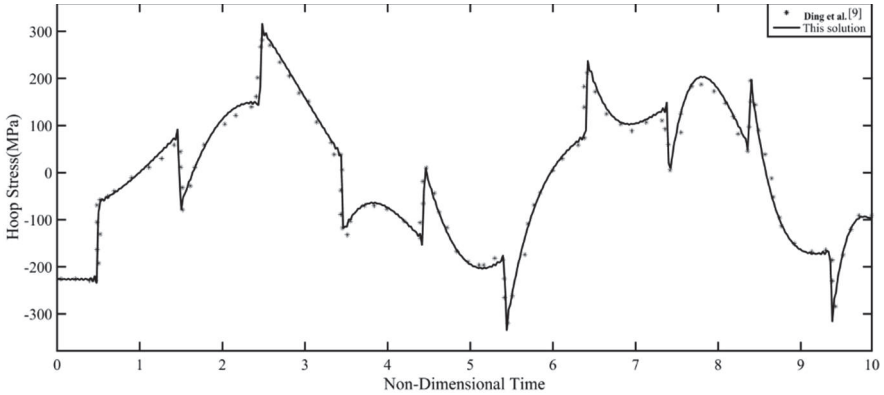

Figure 12 Variation of hoop stress for r = (a+b)/2.

5.2 Coupled Thermoelasticity Problem in Isotropic Cylinder

As is mentioned, isotropic cylinders are special case of orthotropic ones in which there are different material properties in three reference directions. An orthotropic cylinder reduces to isotropic one by selecting same amount for material properties in different directions.

The analytical solution of the fully coupled thermoelasticity problem in isotropic cylinder is recently solved by Sharifi and Shahani [23]. The following properties are employed for comparing the result of the current work with those which obtained for isotropic cylinder.

$$a = 1 \text{ m};\ b = 2 \text{ m};\ \nu = .3;\ \theta_0 = 100^{\circ}\text{C}$$

$$E = 70 \text{ GPa};\ \rho = 2707 \text{ kg/m}^3;\ k = 204 \text{ w/mk}$$

$$\alpha = 23E - 6 \text{ 1/K};\ c = 903 \text{ J/kgK};\ T_0 = 293 \text{ K}$$

The inner surface of the cylinder is subjected to a constant temperature and the outer surface is traction free. Figures 13 and 14 show the history of dynamic radial and hoop stress in cylinder.

Figure 15 shows the temperature difference with respect to the reference temperature. As it can be seen in the figures, selecting the same material properties in different directions for the orthotropic cylinder leads to the same results as in isotropic one.

Comparing the results of the orthotropic cylinder with those plotted for isotropic cylinder, shows significant differences in the amplitude of the figures and the velocity of wave propagation. Considering Figures 6 and 13

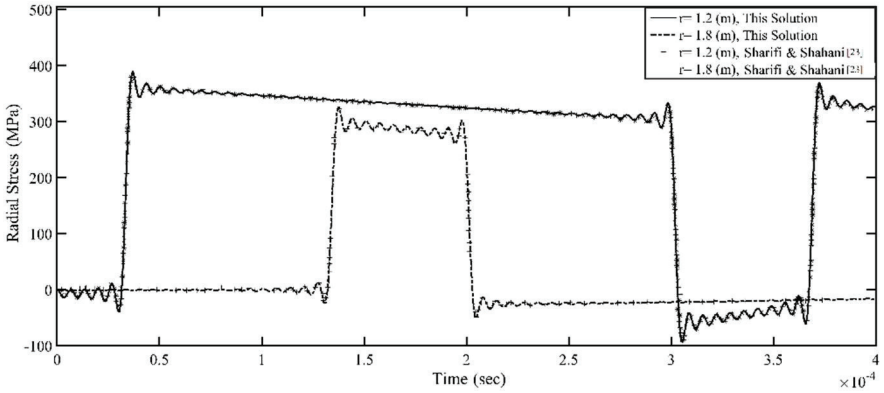

Figure 13 History of dynamic radial stress in isotropic cylinder.

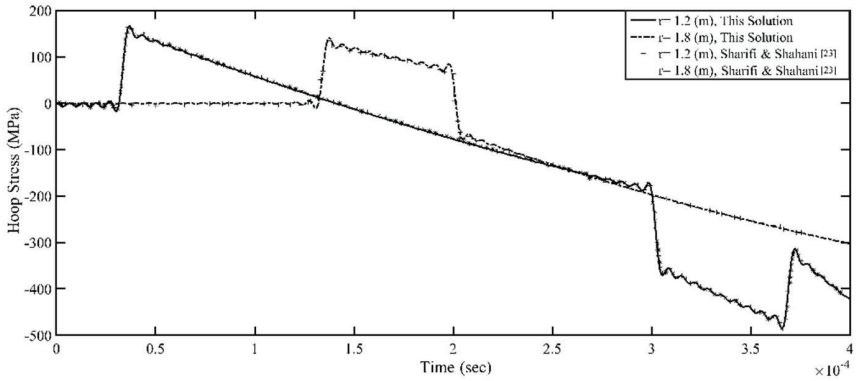

Figure 14 History of dynamic hoop stress in isotropic cylinder.

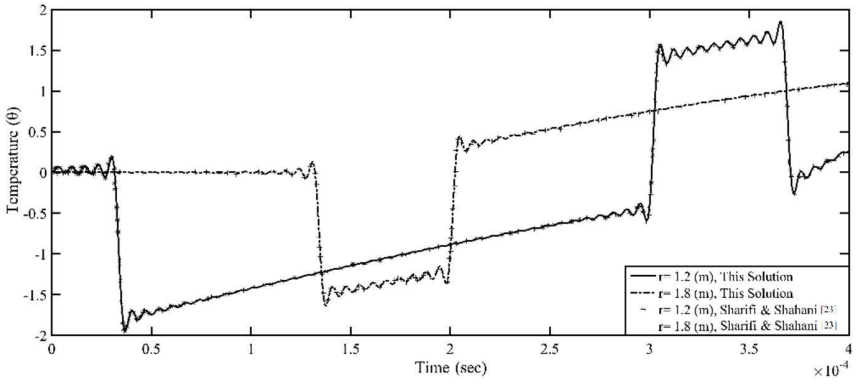

Figure 15 History of temperature in isotropic cylinder.

shows that the maximum radial stress is reduced for the orthotropic case by seven times approximately as well as hoop stresses which are plotted in Figures 7 and 14. In addition the temperature difference which is created due to existence of the coupling term is reduced by half in the orthotropic cylinder.

Velocity of wave propagation in the orthotropic cylinder is less than what it is in the isotropic cylinder. According to this fact it takes more time for the stress wave to reach any radial position in the orthotropic cylinder.

5.3 Orthotropic Cylinder Subjected to a Constant Displacement

As the third verification and to show the power of the presented method, the hypothetical problem of an orthotropic cylinder subjected to a constant displacement is presented. Finite difference method is one of the most common numerical techniques to solve the engineering problems, however, there are lots of complexities in applying the boundary conditions especially the Cauchy (traction) boundary conditions in cylindrical coordinates. For simplicity, a constant displacement of 5 mm is applied on the inner surface of the cylinder, and the outer surface displacement is considered to be zero. The discretization rules for the finite difference method are [29]:

$$\frac{\partial^2 u}{\partial t^2} = \frac{1}{(\Delta t)^2}(u_k^{n+1} - 2u_k^n + u_k^{n-1}) \tag{150}$$

$$\frac{\partial^2 u}{\partial r^2} = \frac{1}{(\Delta r)^2}(u_{k+1}^n - 2u_k^n + u_{k-1}^n) \tag{151}$$

$$\frac{\partial u}{\partial r} = \frac{1}{2\Delta r}(u_{k+1}^n - u_{k-1}^n) \tag{152}$$

And to calculate the displacement at the next time step we have:

$$u_k^{n+1} = 2u_k^n - u_k^{n-1} + d_1 * (u_{k+1}^n - 2u_k^n + u_k^{n-1}) + \frac{d_2}{r_k} * (u_{k+1}^n - u_{k-1}^n) - \frac{d_3}{r_k^2} * (u_k^n) \tag{153}$$

Where:

$$d_1 = \frac{\Delta t^2}{\gamma^2 \Delta r^2} \tag{154}$$

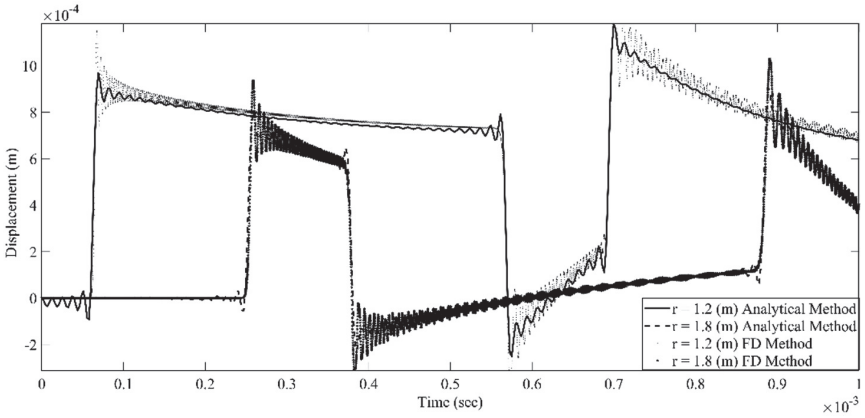

Figure 16 History of displacement in orthotropic cylinder.

$$d_2 = \frac{\Delta t^2}{2\gamma^2 \Delta r} \tag{155}$$

$$d_3 = \frac{\nu^2 \Delta t^2}{\gamma^2} \tag{156}$$

Figure 16 shows the comparison between the results of the finite difference method and the finite Hankel transform for the history of displacement in the hypothetical case of orthotropic cylinder subjected to constant displacement.

It can be seen that the results of the analytical solution are in good agreement with the result of finite difference method.

References

[1] El-Naggar, A.M., et al., Thermal stresses in a rotating non-homogeneous orthotropic hollow cylinder. Heat and Mass Transfer. 39(1) (2002). 41–46.

[2] Shahani, A.R. and S.M. Nabavi, Analytical solution of the quasi-static thermoelasticity problem in a pressurized thick walled cylinder subjected to transient thermal loading. Applied Mathematical Modeling. 31(9) (2007). 1807–1818.

[3] Jabbari, M., H. Dehbani, and M.R. Eslami, An Exact Solution for Classic Coupled Thermoelasticity in Cylindrical Coordinates. Journal of Pressure Vessel Technology. 133(1) (2011). 1–10.

[4] Tokovyy, Y. and C.-C. Ma, Analytical solutions to the axisymmetric elasticity and thermoelasticity problems for an arbitrarily inhomogeneous layer. International Journal of Engineering Science. 92 (2015). 1–17.

[5] Shahani, A.R. and S. Momeni Bashusqeh, Analytical solution of the thermoelasticity problem in a pressurized thick-walled sphere subjected to transient thermal loading. Mathematics and Mechanics of Solids. 19(2) (2014). 135–151.

[6] Shahani, A.R. and S. Momeni Bashusqeh, Analytical Solution of the Coupled Thermo-Elasticity Problem in a Pressurized Sphere. Journal of Thermal Stresses. 36(12) (2013). 1283–1307.

[7] Mahmoudi, H. and G. Atefi, Analytical solution for thermal stresses in a hollow cylinder under periodic thermal loading. Engineering science engineers, part C: Journal of mechanical proceedings of the institution of mechanical. 226(7) (2012). 1705–1724.

[8] Cho, H., G.A. Kardomateas, and C.S. Valle, Elastodynamic Solution for the Thermal Shock Stresses in an Orthotropic Thick Cylindrical Shell Journal of Applied Mechanics. 65(1) (1998). 184–193.

[9] Ding, H.J., H.M. Wang, and W.Q. Chen, A solution of a non-homogeneous orthotropic cylindrical shell for axisymmetric plane strain dynamic thermoelastic problems. Journal of Sound and Vibration. 263(4) (2003). 815–829.

[10] Yun, Y., I.-Y. Jang, and L. Tang, Thermal stress distribution in thick wall cylinder under thermal shock. Journal of Pressure Vessel Technology. 131(2) (2009). 1–6.

[11] Dai, H.-L., Y.-N. Rao, and H.-J. Jiang, Thermoelastic dynamic response for a long functionally graded hollow cylinder. Journal of Composite Materials. 47(3) (2012). 315–325.

[12] Tokovyy, Y., A. Chyzh, and C.-C. Ma, An analytical solution to the axisymmetric thermoelasticity problem for a cylinder with arbitrarily varying thermomechanical properties. Acta Mechanica, (2017). 1–17.

[13] Ying, J. and H.M. Wang, Axisymmetric thermoelastic analysis in a finite hollow cylinder due to nonuniform thermal shock. International Journal of Pressure Vessels and Piping. 87(12) (2010). 714–720.

[14] Nikkhah, M., F. Honarvar, and E. Dehghan, Elastodynamic solution for plane-strain response of functionally graded thick hollow cylinders by analytical method. Applied Mathematics and Mechanics. 32(2) (2011). 189–202.

[15] Safari-Kahnaki, A., S.M. Hosseini, and M. Tahani, Thermal shock analysis and thermo-elastic stress waves in functionally graded thick hollow cylinders using analytical method. International Journal of Mechanics and Materials in Design. 7(3) (2011). 167–184.
[16] Vel, S.S., Exact thermoelastic analysis of functionally graded anisotropic hollow cylinders with arbitrary material gradation. Mechanics of Advanced Materials and Structures. 18(1) (2011). 14–31.
[17] Shahani, A.R. and H. Sharifi Torki, Analytical solution of the thermoelasticity problem in thick-walled cylinder subjected to transient thermal loading. Modares Mechanical Engineering. 16(10) (2016 (inPersian)). 147–154.
[18] Shahani, A.R. and H. Sharifi Torki, Determination of the thermal stress wave propagation in orthotropic hollow cylinder based on classical theory of thermoelasticity. Continuum Mechanics and Thermodynamics. 30(3) (2018). 509–527.
[19] Lata, P. and I. Kaur, Thermomechanical interactions in transversely isotropic thick circular plate with axisymmetric heat supply. Structural Engineering and Mechanics. 69 (2019). 607–614.
[20] Akbarov, S.D. and E.T. Bagirov, The dispersion of the axisymmetric longitudinal waves propagating in the bi-layered hollow cylinder with the initial inhomogeneous thermal stresses. Waves in Random and Complex Media, (2021).
[21] Selvamania, R., S. Mahesha, and F. Ebrahimi, Refined couple stress dynamic modeling of thermoelastic wave propagation reaction of LEMV/CFRP composite cylinder excited by multi relaxation times. Waves in Random and Complex Media, (2021).
[22] Mirparizi, M., A.R. Fotuhi, and M. Shariyat, Nonlinear coupled thermoelastic analysis of thermal wave propagation in a functionally graded finite solid undergoing finite strain. Journal of Thermal Analysis and Calorimetry. 139 (2020). 2309–2320.
[23] Sharifi Torki, H. and A.R. Shahani, Analytical Solution of the Coupled Dynamic Thermoelasticity Problem in a Hollow Cylinder. Journal of Stress Analysis. 5(1) (2020). 121–134.
[24] Jafarzadeh, A., A. Taghvaeipour, and M. Eslami, A Cylindrical Superelement for Thermo-Mechanical Analysis of Thin Composite Vessels. European Journal of Computational Mechanics, (2020). 173–198.
[25] Sharifi, H., Generalized coupled thermoelasticity in an orthotropic rotating disk subjected to thermal shock. Journal of Thermal Stresses. 45(9) (2022). 695–719.

[26] Decolon, C., *Analysis of Composite Structures*. 2002, London: Hermes Penton Ltd.
[27] Sneddon, I.N., *The Use of Integral Transform*. 1972, New York: McGraw-Hill Book Company.
[28] Cinelli, G., An extension of the finite hankel transform and applications. International Journal of Engineering Science. 3 (1965). 539–559.
[29] Gsell, D., T. Leutenegger, and J. Dual, Modeling three-dimensional elastic wave propagation in circular cylindrical structures using a finite-difference approach. The Journal of the Acoustical Society of America. 116(6) (2004). 3284–3293.

Biography

Hamid Sharifi received the bachelor's degree in mechanical engineering from Shahrood University of Technology in 2013, the master's degree in mechanical engineering from K. N. Toosi University of Technology in 2016. He is currently PhD candidate in engineering at Louisiana Tech University, College of Engineering & Science. His research areas include thermoelasticity, elastic wave propagation, and applied mathematics.